Scientific and Social Research, 2025, Volume 7, Issue 5
https://ojs.bbwpublisher.com/index.php/SSR
Online ISSN: 2981-9946
Print ISSN: 2661-4332

Research on the Accuracy of Robot End Position Based on Joint Motion Error

Hualin Zheng[1]*, Yang Liu[1], Yangqiu Xia[2], Xiaobing Hu[3]

[1]School of Mechanical and Electrical Engineering, Southwest Petroleum University, Chengdu 610500, China
[2]National Machine Tool Production Quality Supervision Testing Center, Chengdu 610200, China
[3]School of Mechanical Engineering, Sichuan University, Chengdu 610065, China
**Author to whom correspondence should be addressed.*

Abstract: In robotic intelligent manufacturing engineering, the machining accuracy of workpieces is directly related to the end positioning accuracy of six-degree-of-freedom serial robots, so compensating for the latter is of great significance. This article proposes a method to improve the absolute positioning accuracy of a robot by correcting the joint angles of the robot without changing the parameters of the robot controller. Firstly, establish a forward kinematics model of the robot based on the spiral theory. Then, the motion errors of each joint of the robot are measured using a laser tracker, and the RBF neural network is trained to predict the motion errors of each joint of the robot. Finally, the predicted joint motion errors are compensated for the theoretical joint angles, thereby improving the accuracy of robot end positioning. The experimental results show that the precision of the robot's end position has been improved from 0.2456 mm to 0.0716 mm, verifying the effectiveness of this method.

Keywords: Robot; Joint motion error; Position accuracy; Compensation

Online publication: June 6, 2025

1. Introduction

The motion accuracy of robots is a key factor limiting their performance in high-precision industrial applications [1]. Among the important performance indicators of robots, repeatability and absolute positioning accuracy are the most commonly used metrics [2]. Currently, robots have achieved a relatively high level of repeatability, typically around 0.1 mm. However, the level of absolute positioning accuracy remains significantly lower, generally within the range of 2–3 mm [3]. In order for robots to be effectively applied in precision machining, it is essential to improve their absolute positioning accuracy. Therefore, studying and compensating for the end errors of robots holds significant theoretical importance and practical value.

Currently, there are two primary approaches to improving robot end positioning accuracy: online compensation and offline compensation [4–5]. While online methods can yield high compensation accuracy, they entail high cost, are sensitive to environmental factors (e.g., temperature, humidity, and noise), and lack generality. Offline methods

are more commonly used: they involve error modeling of the robot's kinematic parameters, measurement of the robot end pose using high-precision external instruments, parameter identification based on the error model, and correction of the identified errors in the robot controller to improve positioning accuracy [6]. For example, Filion et al. employed iterative least squares to identify kinematic parameters, improving end accuracy from 0.496 mm to 0.197 mm [7]. Wang et al. combined DH-based modeling with visual measurement and an Extended Kalman Filter (EKF) to estimate and compensate error parameters, achieving approximately 90% improvement in orientation accuracy, though encountering singularity issues [8–9]. Zhu et al. used the Levenberg-Marquardt (LM) algorithm to identify kinematic parameter errors of a dual-arm robot, significantly reducing the average positioning error after compensation [10]. Liu et al. applied the LM algorithm on a UR10 robot, reducing its maximum and average distance errors from 5.60 mm and 2.50 mm to about 0.50 mm and 0.30 mm, respectively [11].

However, these methods require detailed modeling and identification of kinematic-parameter errors, involving complex calculations. Moreover, many industrial robots have closed control systems that do not allow external modification of identified error parameters, rendering compensation infeasible. Literature indicates that joint angle errors account for approximately 90% of the total end error [12–13]. Therefore, reducing joint angle errors can effectively improve robot end positioning accuracy. Some researchers have directly established relationships between Cartesian-space poses and end errors or between joint-space angles and end errors to enhance positioning accuracy. This paper first develops a forward kinematic model of the robot using screw theory, measures each joint's motion error with a laser tracker, and trains an RBF neural network to predict these errors. Based on this, a complete forward-kinematic model is constructed to predict the actual robot end pose. Finally, a single-joint compensation strategy is applied to adjust joint angles and improve robot end positioning accuracy.

2. Theoretical method

2.1. Kinematic modeling based on screw theory

2.1.1. Forward kinematics

Unlike the D-H method, forward kinematic modeling using screw theory does not require establishing a coordinate system at each joint of the robot [14]. Instead, it only requires two coordinate systems: the base coordinate system {S} and the tool coordinate system {T}. Typically, the base coordinate system is connected to the robot's base, and the tool coordinate system is connected to the robot end. Additionally, a screw ξ is associated with each rotational joint [15]. **Figure 1** represents the twist model of the IBR robot. **Table 1** presents the position vectors of specified points on the robot's joint axes.

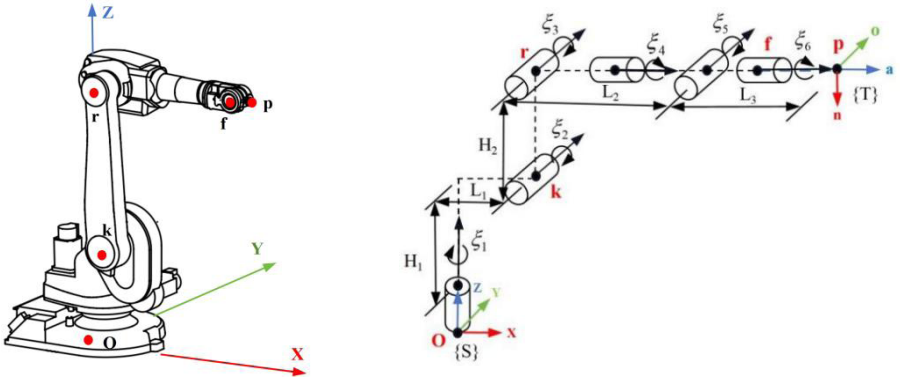

(a) Robot model (b) Robot twist model

Figure 1. 3D model of the robot and its twist model

Table 1. Axis specified point position vector

Vector name	$p(o)$	$p(k)$	$p(r)$	$p(f)$	$p(p)$
Vector value	$\begin{bmatrix}0\\0\\0\end{bmatrix}$	$\begin{bmatrix}L_1\\0\\H_1\end{bmatrix}$	$\begin{bmatrix}L_1\\0\\H_1+H_2\end{bmatrix}$	$\begin{bmatrix}L_1+L_2\\0\\H_1+H_2\end{bmatrix}$	$\begin{bmatrix}L_1+L_2+L_3\\0\\H_1+H_2\end{bmatrix}$

All joints of the robot are rotational joints. $w_i \in R^3$ is the unit vector along the direction of the rotational axis, and $p_i \in R^3$ represents an arbitrary point on the axis. $\boldsymbol{\xi_i} = (-\boldsymbol{w_i} \times \boldsymbol{q_i}, \boldsymbol{w_i})$ is defined as the screw coordinate of the joint, and $\hat{\boldsymbol{\xi}}_{\boldsymbol{i}}$ can be defined as the motion screw of joint i, $\boldsymbol{e^{\hat{\xi}_i\theta_i}}$ is the screw motion of joint i.

$$e^{\hat{\xi}\theta} = \begin{cases} \begin{bmatrix} e^{\hat{w}\theta} & (I - e^{\hat{w}\theta})(w \times v) + \theta w w^T v \\ 0 & 1 \end{bmatrix}, w \neq 0 \\ \begin{bmatrix} I & \theta v \\ 0 & 1 \end{bmatrix}, w = 0 \end{cases} \quad (1)$$

Assuming the initial pose of the robot in the global coordinate system *oxyz* is $g_{st}(0)$, and the unit screw of each rotational joint is $\boldsymbol{\xi_i}$ (i = 1, 2, …, 6), the ideal kinematic equation of the robot end can be expressed as:

$$g_{st}(\theta)_{ideal} = e^{\hat{\xi}_1\theta_1} \cdot e^{\hat{\xi}_2\theta_2} \cdot e^{\hat{\xi}_3\theta_3} \cdot e^{\hat{\xi}_4\theta_4} \cdot e^{\hat{\xi}_5\theta_5} \cdot e^{\hat{\xi}_6\theta_6} \cdot g_{st}(0) \quad (2)$$

2.1.2. Inverse kinematics

In inverse kinematics, given the robot end pose of the robot, the joint angles can be obtained by solving the Paden-Kahan subproblem. For the IRB robot in this study, which has a special configuration with multiple parallel joint axes, the inverse kinematics is decomposed into several Paden-Kahan subproblems and Paden-Gahan subproblems for solving [16]. Taking the robot shown in **Figure 1** as an example, inverse kinematics is solved using screw theory.

First, the values of θ_1, θ_2, and θ_3 are solved using the PG7 subproblem. According to screw theory, the point q located on the axis of rotation remains stationary regardless of the rotation angle, i.e.

$$e^{\hat{i}\dot{e}} q = q \quad (3)$$

Therefore, by multiplying both sides of equation (2) by $g_{ST}(0)^{-1} f$ (where f is the intersection point of the last three joints), get:

$$e^{\hat{i}_1\dot{e}_1} \cdot e^{\hat{i}_2\dot{e}_2} \cdot e^{\hat{i}_3\dot{e}_3} \cdot e^{\hat{i}_4\dot{e}_4} \cdot e^{\hat{i}_5\dot{e}_5} \cdot e^{\hat{i}_6\dot{e}_6} \cdot f = g_{\boldsymbol{S}}(\dot{e}) g_{\boldsymbol{S}}(0)^{-1} f \quad (4)$$

It can be simplified as follows:

$$e^{\hat{i}_1\dot{e}_1} \cdot e^{\hat{i}_2\dot{e}_2} \cdot e^{\hat{i}_3\dot{e}_3} \cdot f = g_{\boldsymbol{S}}(\dot{e}) g_{\boldsymbol{S}}(0)^{-1} f = p_1 \quad (5)$$

The right-hand side of the equation is a known quantity, denoted as P_1. By solving the PG7 subproblem, the angles of the first three joints can be obtained. Similarly, the values of θ_4, θ_5, and θ_6 can be solved through the PG6 subproblem and the Pk1 subproblem, respectively.

Given the robot end pose of a six-degree-of-freedom robot, the inverse kinematics can yield 8 sets of inverse solutions, each corresponding to a different motion posture of the robot. Based on the principle of minimizing joint movement, the appropriate set of inverse solutions is selected in this study.

2.2. Identification of joint motion errors

2.2.1. Robot joint motion errors

As shown in **Figure 1**, all joints of the robot are rotational joints, and their motion errors mainly manifest as joint angle errors Δθ, which represents the difference between the ideal joint angle θ and the actual joint angle θ′ of each joint. These errors directly affect the robot's volumetric errors, causing the actual robot end pose to deviate from the ideal pose. During the robot's actual motion, the joint motion errors change as the corresponding joint rotation angle varies, meaning they are dependent on the magnitude of the joint rotation angles.

Although the motion errors of each joint are small, the cumulative errors from multiple joints can significantly increase the robot end pose error, especially in high-degree-of-freedom robots or complex motion paths. The impact of joint motion errors on the robot end volumetric errors is shown in **Figure 2**.

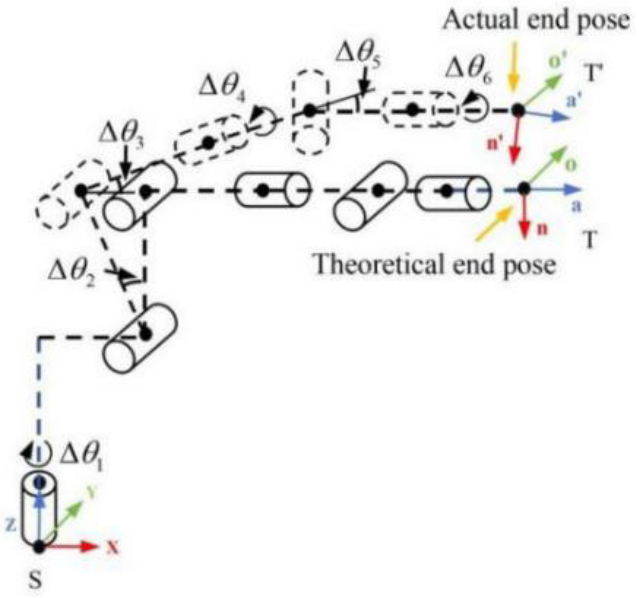

Figure 2. The influence of joint motion error on the end errors of the robot

2.2.2. Joint motion errors measurement using a laser tracker

There are many instruments for identifying robot joint motion errors, among which the laser tracker is a commonly used measurement tool. When using a laser tracker to measure joint motion errors, one joint of the robot rotates while keeping the other joints fixed. The rotating joint changes its angle incrementally, and the laser tracker continuously tracks the position of the robot end target ball in real time. After each movement, the robot returns to the zero position, as shown in **Figure 3**.In this setup, assuming the ideal position of any selected point within the robot's motion range in the robot's base coordinate system is $p_i(i=1,2\ldots n)$, and its coordinates in the laser tracker coordinate system are , the following expression can be obtained:

$$p_i = Q^{-1} \cdot (p_i' - T) \tag{6}$$

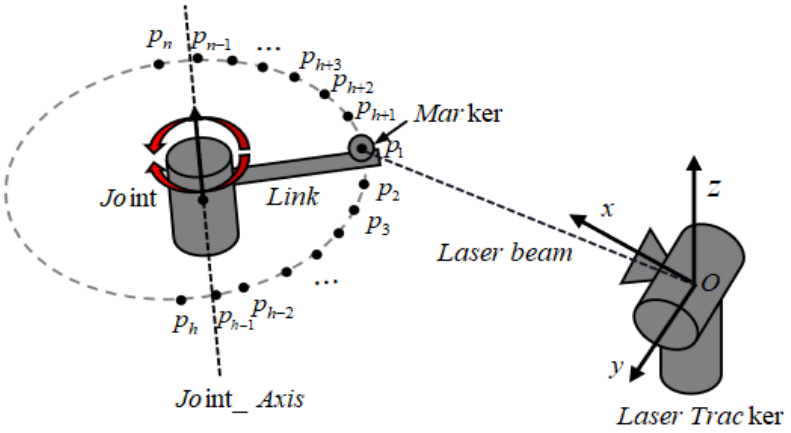

Figure 3. Measurement of joint motion errors using a laser tracker

where T is the translation vector, and Q is the rotation matrix between the robot coordinate system and the laser tracker coordinate system. A method for obtaining this matrix is proposed in reference [17]. By transforming the measurement points in the laser tracker coordinate system to the robot coordinate system, and knowing the ideal robot end position of the robot, the actual joint rotation angles can be solved through the rotation center.

3. RBF neural network for error prediction

The joint motion error data of the robot measured by a laser tracker consists of discrete points. A neural network is used to perform data fitting on this information. The joint angles are used as the input variables, and the motion errors are used as the output variables to train the neural network, enabling the prediction of motion errors corresponding to any given joint angle.

The Radial Basis Function (RBF) consists of three layers: the input layer, hidden layer, and output layer, as shown in **Figure 4** [18]. Its working principle involves using symmetric functions to convert multivariate problems into univariate approximation problems. At present, RBF networks are commonly used in fields such as numerical approximation and image processing.

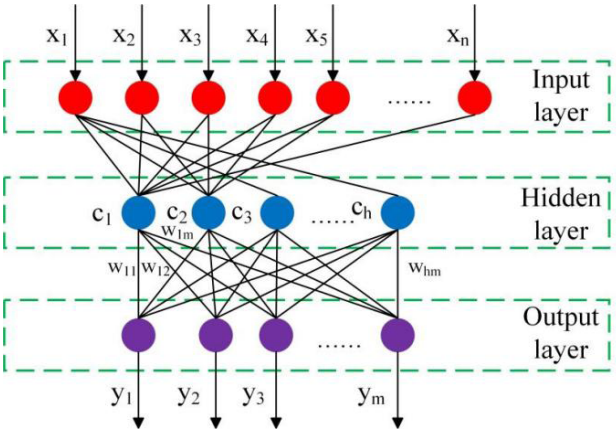

Figure 4. Schematic diagram of RBF neural network

The Radial Basis Function (RBF) neural network offers a variety of activation functions. In this study, the Gaussian function is employed as the activation function of the network. Its output expression is given as follows:

$$y_j = \sum_{i=1}^{h} w_j e^{(-\frac{\|x_k - c_i\|^2}{2\sigma^2})} \tag{7}$$

In the above expression, $x = [x_1, x_2 \cdots x_n]^T$ denotes the input vector, $y = [y_1, y_2 \cdots y_m]^T$ represents the output, w_{ij} is the weight matrix, and $c = [c_1, c_2 \cdots c_h]^T$ indicates the center of the hidden layer nodes. The term also represents the variance between the expected and actual outputs of the sample, which is defined as follows:

$$\sigma = \frac{1}{n} \sum_{j=1}^{m} \left\| d_j - y_j c_i \right\|^2 \tag{8}$$

In this expression, i=1,2…h denotes the number of hidden layer nodes, i=1,2…m represents the number of network outputs, k=1,2…n is the number of network inputs, and d corresponds to the expected output of the sample. In this study, joint angles are used as the input variables x and the corresponding joint motion errors as the output variables y to train the neural network, enabling the prediction of motion errors for arbitrary joint angles.

In summary, this study first establishes the robot's forward kinematic model based on screw theory. Then, joint motion errors are measured using a laser tracker, and an RBF neural network is trained to predict the motion error corresponding to any given joint angle. Next, a set of discrete points along the robot end trajectory is designed to obtain the ideal robot end poses. Using the inverse kinematic model, the corresponding ideal joint angles are calculated, and the predicted joint motion errors are compensated for in these angles to improve robot end positioning accuracy. Finally, a ball-bar instrument is employed to verify the enhancement in end positioning precision.

4. Experiment and analysis

This section validates the effectiveness of the robot end volumetric errors optimization compensation method through experiments. The test subject is an IRB1600 industrial robot (6 axes, 10 kg payload, 1450 mm working range, repeatability accuracy of ±0.05 mm). The robot operates under a rated load of 0.02 kg, as shown in **Figure 5**. The robot parameters used for screw theory modeling are listed in **Table 2**.

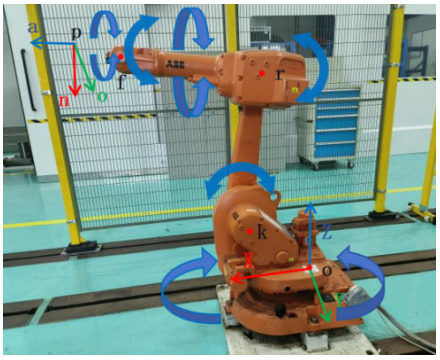

Figure 5. Industrial robot

Table 2. Robot parameters for screw theory modeling

Joint	$e^{\hat{\xi}_1\theta_1}$	$e^{\hat{\xi}_2\theta_2}$	$e^{\hat{\xi}_3\theta_3}$	$e^{\hat{\xi}_4\theta_4}$	$e^{\hat{\xi}_5\theta_5}$	$e^{\hat{\xi}_6\theta_6}$
ω	$[0\ 1\ 0]^T$	$[0\ 1\ 0]^T$	$[0\ 1\ 0]T$	$[1\ 0\ 0]^T$	$[0\ 1\ 0]^T$	$[1\ 0\ 0]^T$
p	$\begin{bmatrix}0\\0\\0\end{bmatrix}$	$\begin{bmatrix}0.15\\0\\0.4865\end{bmatrix}$	$\begin{bmatrix}0.15\\0\\1.1865\end{bmatrix}$	$\begin{bmatrix}0.75\\0\\1.1865\end{bmatrix}$	$\begin{bmatrix}0.75\\0\\1.1865\end{bmatrix}$	$\begin{bmatrix}0.815\\0\\1.1865\end{bmatrix}$
v	$q\times w$	$q\times w$	$q\times w$	$q\times w$	$q\times w$	$q\times w$
θ	θ_1	θ_2	θ_3	θ_4	θ_5	θ_6

4.1. Joint motion error identification

Using the measurement method described in Section 2.2, the joint motion errors of the robot are identified. The robot is kept at its zero position, and starting from the first joint, a target point is selected every 5° within the robot's motion range. A laser tracker is used to measure the target ball position as the joint moves from the zero position to the target point. Each target point is measured three times. Once the data for the first joint target points are collected, the robot returns to the initial zero position and the measurements for the next joint are performed sequentially. The experimental setup is shown in **Figure 6**.

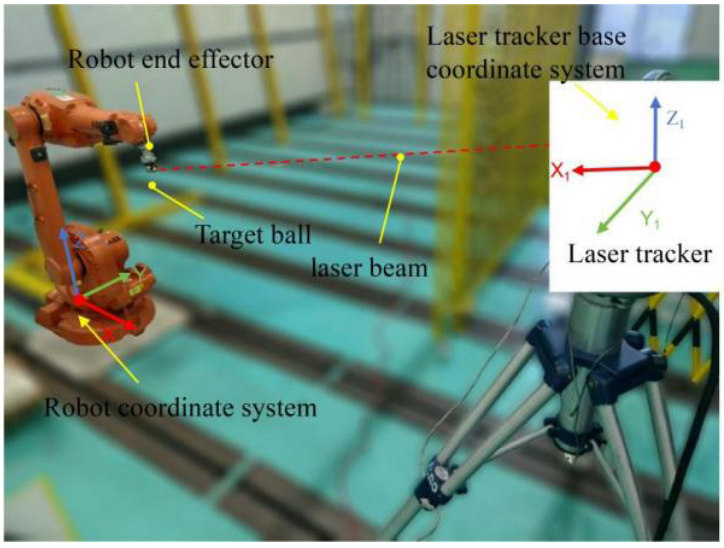

Figure 6. Laser tracker measures the motion error of each joint of the robot

The data measured by the laser tracker are trained using the RBF neural network from Section 2, and the training results are shown in **Figure 7**. By inputting the joint angles of the robot, motion errors for any given joint angle within the robot's motion range can be predicted.

As shown in **Figure 7**, the motion errors of joints 2 and 4 tend to increase as the joint angles increase, while the motion errors of joints 3 and 5 decrease as the joint angles increase. The motion errors of joints 1 and 6 stabilize as the joint angles increase.

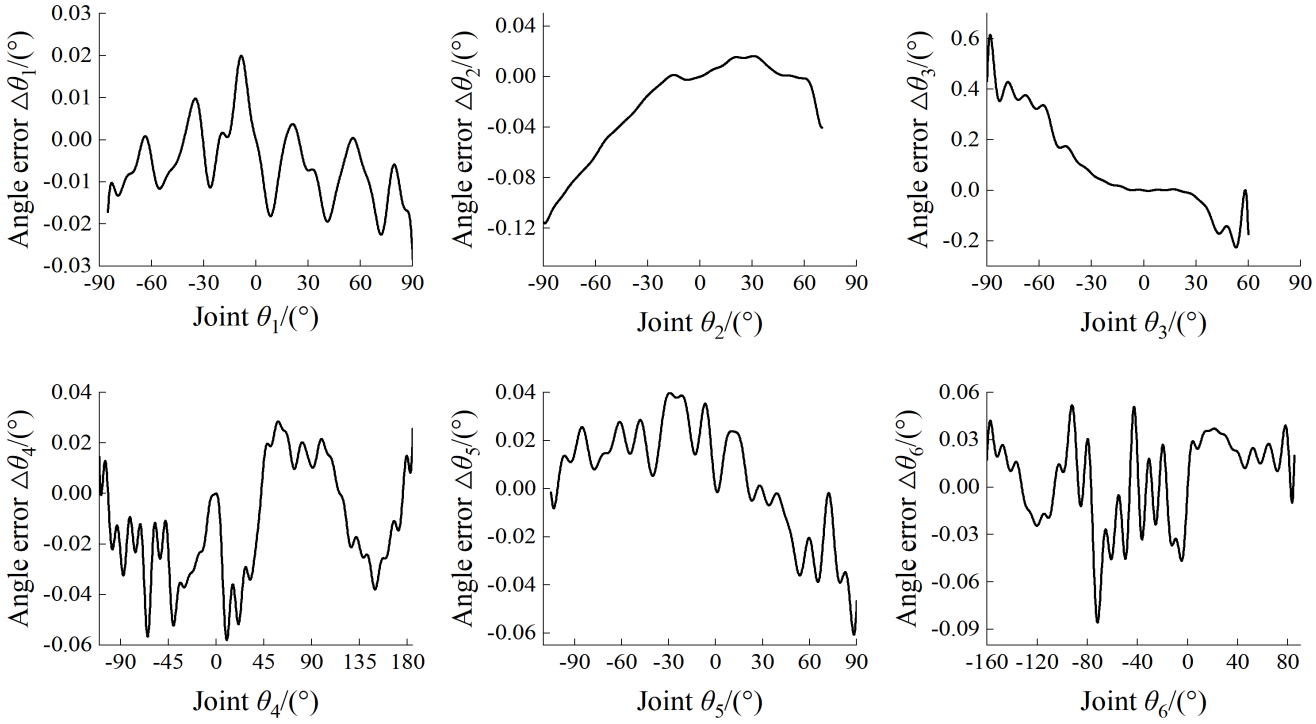

Figure 7. Distribution diagram of joint motion error

4.2. Verification of robot end position error compensation

To evaluate the effectiveness of joint motion error compensation on the robot end positioning accuracy, a ball-bar system was used to measure the end position error. First, a set of discrete points along the desired robot end trajectory was designed, as shown in **Figure 8**. Given the ideal pose at each trajectory point, the corresponding ideal joint angles were calculated using inverse kinematics. The ball-bar tool cup was mounted to the robot end, and the robot was programmed to follow a semicircular path in a 45° inclined plane through the predefined discrete points. The variation in ball-bar length at each point was recorded to assess the positioning accuracy. The experimental setup and the measured length variations are shown **in Figures 9(a)** and **9(b)**, respectively.

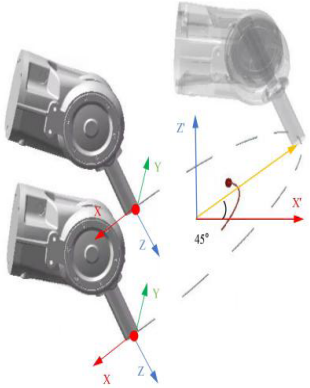

Figure 8. Design of discrete points for robot end trajectory

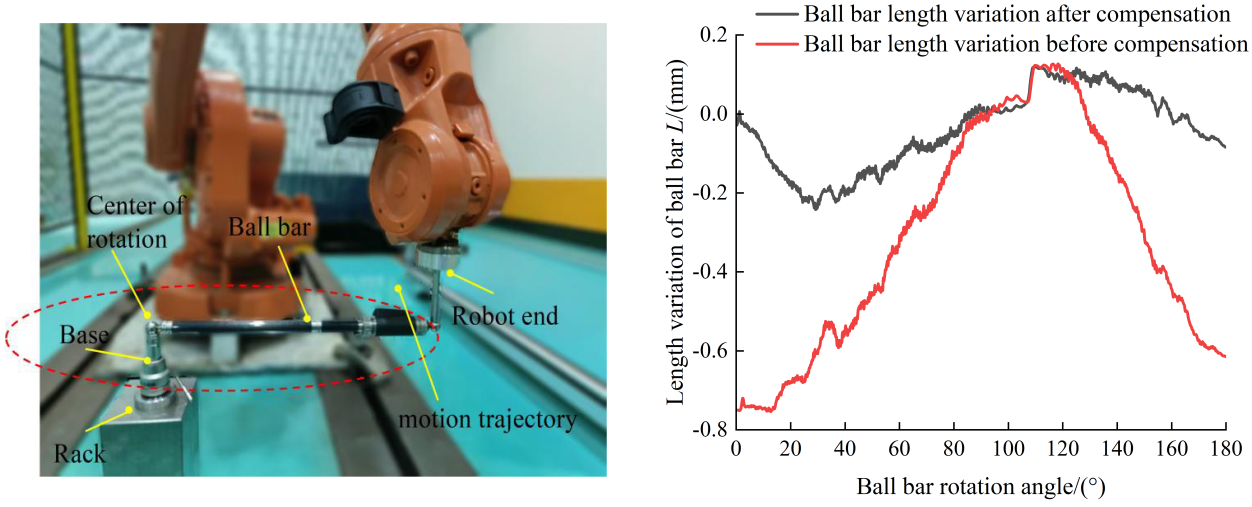

(a) Experimental setup

(b) Length variation of ball bar

Figure 9. Identification of robot end position accuracy with ball rod instrument

As shown by the compensation results in **Figure 9**, before error correction, the ballbar length varied by a maximum of 0.7582 mm with a mean of 0.2456 mm. After incorporating the identified joint motion errors into the robot's actual joint angles, the maximum length variation decreased to 0.2593 mm and the mean to 0.0716 mm. Consequently, the robot end positioning accuracy improved from 0.2456 mm to 0.0716 mm [19].

5. Conclusion

This paper proposes a method to improve the absolute positioning accuracy of the robot end by correcting the joint angles of the robot without changing the parameters of the robot controller. The experimental results show that the end position accuracy of the robot has been improved from 0.2456 mm to 0.0716 mm after joint motion error compensation, which verifies the feasibility of the error compensation method proposed in this paper in robot position accuracy compensation.

Disclosure statement

The authors declare no conflict of interest.

References

[1] Yang P, Guo ZG, Kong YB, 2020, Plane Kinematic Calibration Method for Industrial Robot Based on Dynamic Measurement of Double Ball Bar. Precision Engineering, 2020(62): 265–272.

[2] Lv ZY, Wen XL, Cui WX, et al., 2021, Research on Pose Point Set Optimization for Kinematic Parameter Calibration of Industrial Robots. Instrument Technique and Sensor, 2021(7): 97–102 + 121.

[3] Liu W, Liu S, Deng Z, et al., 2023, Research Progress on Positioning Error Compensation Technology of Industrial Robot. Journal of Mechanical Engineering, 59(17): 1–16.

[4] Xue L, Yang YK, Li DS, et al., 2024, Identification and Online Compensation Method of Robot End Load Gravity Based on Laser Tracker. Aviation Manufacturing Technology, 67(5): 53–59.

[5] Jiao JC, Tian W, Zhang L, 2022, Hierarchical Compensation Technology for Machining Error of Industrial Robots. Computer Integrated Manufacturing System, 28(6): 1627–1637.

[6] Ding C, Zhao RH, Li L, et al., 2020, Research on the Accuracy of Robot End Position Based on Joint Angle Deviation. Micro Nano Electronics and Intelligent Manufacturing, 2020(3): 30–35.

[7] Filion A, Wang XL, Liu ZHF, et al., 2019, New Method for Robot Tool and Camera Pose Calibration. Chinese Journal of Scientific Instrument, 40(1): 101–108.

[8] Pu ZW, Cao BS, Xie ZW, et al., 2023, Kinematic Calibration of a Space Manipulator Based on Visual Measurement System with Extended Kalman Filter. Machines, 2023(11): 409.

[9] Mi X, Ku XC, Ma DY, et al., 2022, Singularity Analysis of 6R Articulated Robot. Journal of Mechanical & Electrical Engineering, 39(11): 1620–1626.

[10] Zhu QD, Xie XR, Li C, et al., 2019, Kinematic Self-calibration Method for Dual-Manipulators Based on Optical Axis Constraint. IEEE Access, 2019(7): 7768–7782.

[11] Liu Y, Zhuang ZH, Li YW, 2022, Closed-Loop Kinematic Calibration of Robots Using a Six-Point Measuring Device. IEEE Transactions on Instrumentation and Measurement, 2022(71): 1–12.

[12] Judd RP, Knasinski AB, 1990, A Technique to Calibrate Industrial Robots with Experimental Verification. IEEE Transactions on Robotics and Automation, 6(1): 20–30.

[13] Zhang L, Tian W, Zheng FW, 2020, Accuracy Compensation Technology of Closed-Loop Feedback of Industrial Robot Joints. Transactions of Nanjing University of Aeronautics and Astronautics, 37(6): 858–871

[14] Zhang YJ, Cui J, Li Y, et al., 2023, Modeling and Calibration of High-order Joint-dependent Kinematic Errors of Serial Robot Based on Local POE. Industrial Robot-The International Journal of Robotics Research and Application, 50(5): 753–764.

[15] Gao WB, Luo RQ, Jian, ZZ, 2021, Kinematic-Parameter Calibration for Modular Robots Based on the Local POE. Jiqiren/Robot, 43(1): 66–73.

[16] Pardos-Gotor J, 2021, Screw Theory in Robotics: An Illustrated and Practicable Introduction to Modern Mechanics. CRC Press, Florida.

[17] Zhang B, Wei ZZ, Zhang GJ, 2010, Fast Conversion Method Between Robot Coordinate System and Laser Tracker Coordinate System. Journal of Instrumentation and Instrumentation, 2010(9): 1986–1990.

[18] Liu YC, Xiong YH, Yang HX, 2022, Fixed-time Sliding Mode Control of Multi-joint Robot Based on RBF Neural Network. Control and Decision, 37(11): 2790–2798.

[19] Che YX, Yang XG, Gao F, 2017, Research on Kinematic Calibration Method of Three Degree of Freedom Serial Robot Arm Based on Ball Rod Instrument. Mechanical Strength, 39(6): 1315–1319.